Fabrication of sulfur cathodes by wet-powder spraying and the understanding of degradation

Natalia A. Cañas[a], *Ana L. P. Baltazar*[a‡], *Micael A. P. Morais*[a‡], *T. Oliver Freitag*[a], *N. Wagner*[a,1], *K. Andreas Friedrich*[a,b]

[a]Institute of Engineering Thermodynamics, German Aerospace Center, Stuttgart, Germany

[b]Institute for Thermodynamic and Thermal Engineering, University of Stuttgart, Germany

[‡]These authors contributed equally to this work.

[*]Corresponding author at: Institute of Technical Thermodynamics, German Aerospace Center, Stuttgart, Germany.

Tel.: +49 711 6862 576; Fax: +49 0711 6862 474.

E-mail addresses: natalia.canas@dlr.de, nataliacanas@gmail.com

[1]Electrochemical Society Active Member.

Abstract

In this work, wet powder spraying is presented as an alternative method for the fabrication of sulfur/carbon composite cathodes. The high dispersion and homogeneity of the cathode layer result in high capacity Li/S batteries. Additional use of $LiNO_3$ as additive improved the energy density to 800 Ah kg_S^{-1}, 400 Ah $kg_{cathode}^{-1}$ (at 0.18 C) and 410 Ah kg_S^{-1}, 205 Ah $kg_{cathode}^{-1}$ (at 2 C) after 50 cycles. The shuttle mechanism is reduced and a coulombic efficiency of around 100% is reached and

maintained constant until 1000 cycles. To understand more the degradation mechanisms of the battery, Thermogravimetry combined with gas analysis (TG/MS) as well X-ray diffraction (*operando* and mappings) were applied. The formation of an amorphous phase during cycling that remains nearly stable in the later cycles is considered to be one of the main factors affecting capacity decay. Moreover, others processes are identified as contributors of battery degradation like PVDF decomposition, structural changes of carbon black, and reduction of sulfur content on the bulk of the electrode. These new insights on the degradation processes may contribute to the further understanding, selection of materials, and improvement of this battery.

1. Introduction

Li/S batteries present many advantages including a high theoretical capacity (1675 Ah kg^{-1}), high energy density (2500 Wh kg^{-1}), and low cost of sulfur. However, degradation of the battery components at high number of cycles and high discharge rates is still a problem. The development of components and fabrication processes applicable at large-scale production and at low cost is also a great challenge for the commercialization of Li/S batteries.

Most attempts to improve the electrochemical performance of Li-S batteries have been focused on the positive electrode [1–4]. Due to the low electrical conductivity of sulfur, the incorporation of a conductive material in the cathode of Li-S batteries is one of the main issues related to the fabrication of the electrode. Different strategies were developed associated to the selection of the conductive material and the method of incorporating sulfur in the composite. Carbon black [5–12], active carbon [13,14] carbon nanotubes [5], and graphene [15,16] are common conductive materials applied in Li-S batteries. The sulfur

composite is prepared by mechanical mixing/milling of both components, by melting or sublimation of sulfur, or by *in situ* reaction of sulfur. These last strategies facilitate the incorporation of sulfur in nano materials. The incorporation of sulfur in a nano-porous conductive matrix were first presented by Wang and coworkers [13,14]. The pore size was around 2.5 nm and resulted in batteries with a reversible capacity of 400 Ah kg_S^{-1} (current density: 0.3 mA cm^{-2}, max. 25 cycles). Ji and coworkers [17] obtained better cyclability with the utilization of high order meso-porous carbon; 6.5 nm diameter carbon tubes separated by 3-4 nm wide channel voids. This configuration should help to trap the polysulfides and facilitate the conduction of ions and electrons in the matrix. Reversible capacity of 1005 Ah g_S^{-1} was achieved (current density: 0.37 mA cm^{-2}, max. 20 cycles). Further attempts were made using the same approach to encapsulate sulfur in an conductive matrix , among others: [18–21].

Li-S batteries fabricated by Wang and coworkers [22] achieved discharge capacities of 800 Ah kg_S^{-1} up to 400 cycles at a discharge rate of 0.2 C. They created hollow carbonized polypyrolle spheres of around 450 nm diameter, in which melted sulfur was embedded. Stable capacities (~400 Ah kg^{-1}) at 2 C were demonstrated by Fu et al. using a sulfur polypyrrole composite cathode [23]. High cycling performance until now were demonstrated by Seh and colleagues [3]. They generated a TiO_2 yolk shell with internal void to encapsulate sulfur and retain intermediate products. This configuration showed capacity retention of 67 % after 1000 cycles.

In this work, we present developments related with the fabrication of industrially-oriented cathodes, the main factors affecting the battery capacity, and new insights into the degradation processes of the Li-S battery. Wet powder spraying technique is presented as an alternative method to doctor blade that can be applied successful for the fabrication of sulfur/carbon composites electrodes. Moreover, the degradation of

sulfur/carbon composites cathodes are studied with a) X-ray diffraction for detection and quantification of crystalline and amorphous products and b) Thermogravimetry coupled with mass spectroscopy (TG/MS) to study the degradation of components and prove the morphological changes on the cathode.

2. Experimental

2.1 Cathode preparation

The cathode were composed of 50 wt.% sulfur powder (S, 99.5% purity, Alfa Aesar), 40 wt.% Super P carbon black (CB, 99% purity, Alfa Aesar) as conductive material, and 10 wt.% polyvinylidene fluoride (PVDF, Alfa Aesar) as binder. PVDF was dissolved separately in a 50/50 vol.% mixture of DMSO and ethanol. Ethanol was added to facilitate the transport of the cathode suspension in the spraying machine and for rapid evaporation after coating.

Two different cathodes are compared in this work according with the fabrication steps summarized in Table A.1. The main differences were: (a) Cathode I was prepared by mixing the powder components in a roll mixer and afterward the solvents were added. The suspension was sprayed using an internal nozzle and coated in one step, while the substrate was placed in a heating plate at 100°C. (b) Cathode II was prepared by mixing S and CB in a tumbling mixer at higher velocity and by adding later the PVDF dissolved in DMSO/Ethanol. The coating process was carried out in three steps; between each spraying, the cathode was dried in an oven at 60 °C. The reduction of temperature avoided the formation of cracks in the layer due to rapid drying. Spraying in three steps, by addition of drying steps between each coating, improved the stability of the cathode and the adherence on the aluminum, and the homogeneity of the layers (Cathode II).

The thickness of the cathode layer, without substrate, varied between 15-20 µm. The sulfur loading was 0.45 mg cm^2 and density of the active layer 0.13 mg cm^{-3}. These values can be increased by raising the sulfur content in the composite. The thickness of the electrode can be increased according with demand, by inclusion of furthers spraying/drying steps. However, the electrode thickness is limited by the diffusional resistance or loss of adhesion of the active layer with the substrate. Lower sulfur utilization is observed in Li-S batteries for sulfur cathodes with increasing cathode thickness or sulfur loading [24]; and the formation of discharge and charge products may be concentrated at the surface of the electrode. The use of protective and stabilizer layers may be necessary to avoid high capacity decay due to the higher content of low conductive sulfur [25–27]. Here, we are presenting the wet powder spraying method for coating of sulfur/carbon composites. However, improvements on the capacity stability and increase in the total specific energy are still part of the ongoing work. Using a wet powder spraying machine, the cathode suspension was applied onto a substrate with pressurized air. The suspension was placed in a pressurized tank and it was directed to the nozzle inside a polypropylene tube. An air-atomizing external mixing nozzle (LECHLER GmbH) was used for this purpose, and the slurry mixes with the air outside the nozzle. The movement of the nozzle as well as the sample holder was controlled by a 3D axis robot (Janome JR 2400N GLT). The axis with the nozzle moves in perpendicular direction (y) to the substrate holder at 300 mm s^{-1}, while the substrate holder advances step by step in x-direction so all the surface of the substrate is coated. The pressure of air and suspension, as well the distance between nozzle and layer, were adjusted to obtain a uniform spraying. Homogenous layers were obtained by injecting the suspension at low pressures (between 0.2-0.4 bar) and atomizing externally with air at 0.5 bar pressure. The distance between nozzle and substrate was set at z = 180 mm.

After drying the cathode were punched out for cell preparation in individual cathodes of 10 and 16 mm diameter.

2.2 Cell construction and electrochemical testing

The battery was built and tested in a so-called Swagelok® cell to assure the hermetic sealing and to avoid reaction of the battery components with air according to the procedures previously published.[28,29] Cathodes of 10 and 16 mm diameter were tested. The volume of electrolyte was maintained constant for all tested cells (14 and 36 µL for small and large cells respectively) as well as the concentration of $LiPF_6$ (1 M) in TEGDME. Electrolytes with different $LiNO_3$ concentration (0, 0.1, 0.5, 0.75, and 1 M) (99.99%, Sigma-Aldrich) were prepared in the glove box under Ar atmosphere using a magnetic stirrer for at least 24 hr. A 0.75 mm thick lithium foil (99.9%, Sigma-Aldrich) was used as anode, and Celgard® 2500 as separator.
The electrochemical testing or cycling of the batteries was carried out with a cell test system (BaSyTec) [30]. The charge-discharge proceeded galvanostatically at 300 A kg_{sulfur}^{-1} (0.18 C). The battery was first discharged until 1.5 V, charged at constant current density up to 2.8 V, and then a potentiostatic period followed for 15 min before starting the next cycle.

2.3 Characterization procedures

Samples were measured in a simultaneous thermal analysis (STA) equipment (Netzsch, STA 449C Jupiter®)) coupled with a mass spectrometer (MS) (Netzsch, MS403C). A plate crucible made of Al_2O_3 (T_{max}=1700°C), with a diameter of 17 mm, was chosen for measuring the samples in order to place the 16 mm diameter cathodes over it without being cut. The samples were heated from 25°C until 1000°C at a constant

heating rate of 5 K min^{-1}. The gas used for the experiments was a 20:80 mixture of O_2/N_2. The gases generated during heating were analyzed in line with the mass spectrometer. First, the cathode components: carbon black (CB), polyvinylidene fluoride (PVDF) and sulfur (S) were analyzed separately and second, the cathodes before and after cycling were measured after drying.

X-ray diffractograms were recorded using an x-ray diffractometer (D8 Discover Bruker GADDS) with a VÅNTEC-2000 detector. The spectra were taken on reflection mode using a tuned monochromatic and parallel x-ray beam (Cu-K_α). The accelerating voltage was 45 kV and the tube current was 0.650 mA. An XRD mapping was measured using the raster grid schematically shown in Fig. 7 (a). The cathode was measured in 13 positions and during the measurement the sample stage oscillated in 0.5 mm XY to obtain higher statistic information of the sample.

3. Results and discussion

3.1 Influence of cathode fabrication on the capacity fading

High resolution SEM pictures show that the uses of different fabrication procedures result in dissimilar cathode morphologies (Fig. A.1). Cathode I presents larger particle size (up to ca. 20 µm) than Cathode II. Moreover, no homogenous particle size is obtained in Cathode I, probably because of the agglomeration of S crystallites due to soft mixing produced by the roll mixer. On the other hand, the tumbling mixer reduces the sulfur particle to less than 4 µm, and only some larger particles are present. Moreover, Cathode II has a surface completely covered by CB particles. Some CB particles seem to be embedded in the sulfur and some wrapped around the sulfur. The CB network and the close contact between the conductive carbon and sulfur are

responsible for providing electron pathways for the insulating sulfur. In case of Cathode I, the uncovered area of sulfur particle is higher.

Fig. 1 shows the discharge capacity vs. cycle number for Cathode I and Cathode II with the electroltyte: 1 M $LiPF_6$ in TEGDME. The discharge capacity is based on the mass of sulfur present in the battery. Batteries fabricated with Cathode II have a higher discharge capacity, in the first cycle 1150 Ah kg_S^{-1} compared to 850 Ah kg_S^{-1} for Cathode I. The reversible discharge capacity after 50 cycles remains at 528 Ah kg_S^{-1} while for Cathode I is 275 Ah kg_S^{-1}, this represents 32% and 47% capacity retention respectively. The Coulombic efficiency is in both cases not stable during cycling with values lower than 100%. The high values of the error bars demonstrate the instability of the batteries due to the charge process. The improved dispersion of S particles, the high contact with carbon black network, as well as the reduction of S particle size, are responsible for the increase in the discharge capacity of batteries fabricated with Cathode II. This is related to a higher active surface area which enhances sulfur dissolution and utilization for the electrochemical reactions. Nevertheless, both systems display similar capacity retention. This means that the reduction of particle size and increase of particle dispersion influence positively the utilization of the active material in the first cycles but it does not avoid the capacity fading of the batteries.

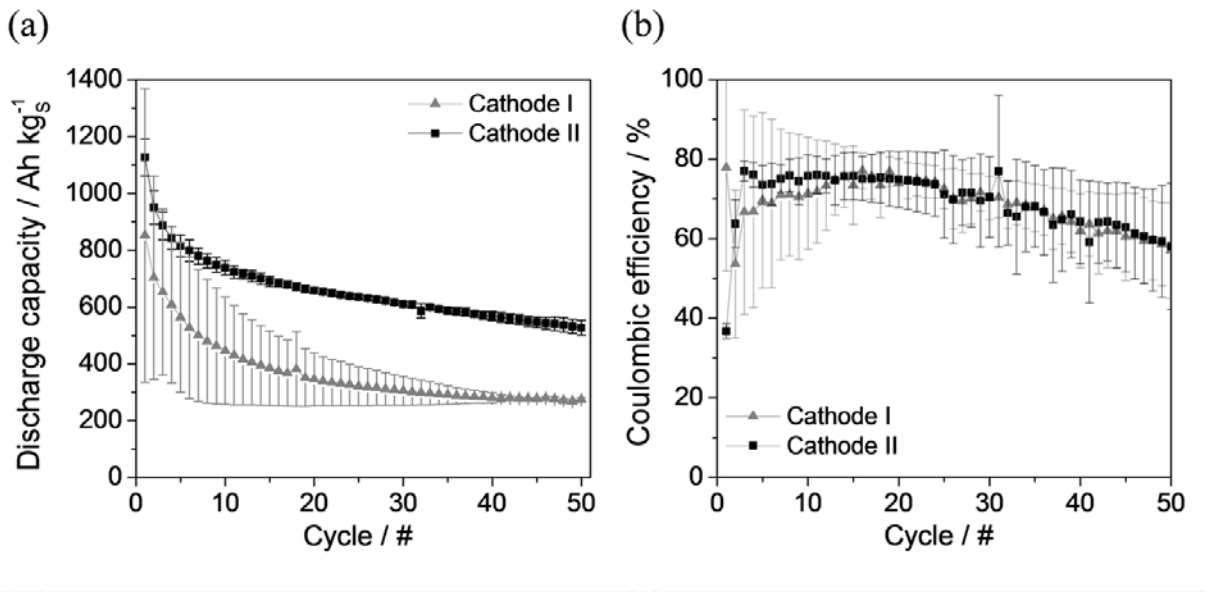

Fig. 1 : Cyclability of batteries using Cathode I and Cathode II at 0.18 C-rate. (a) Discharge capacity vs cycle. (b) Coulombic efficiency. Electrolyte: 1 M $LiPF_6$ in TEGDME. Three cells were tested for each type of cathode. The average and error bars are calculated based on the results of 3 tested batteries

The shuttle effect is observed during charge and originates an increase of the charge capacity that varies from cell to cell (see discharge curves Fig. A.4). The large errors bars shown in Fig. 1 (b) are the result of the difference in charge capacity. On the one hand, Li_2S is oxidized in the cathode generating long-chain lithium polysulfides and elemental sulfur step by step. On the other hand, polysulfides are reduced chemically on the lithium surface. When the concentration of long-chain lithium polysulfides increases, the shuttle phenomenon is enhanced. Thus, at the high plateau (~ 2.5 V) two processes would be in competition: the electrochemical oxidation of polysulfide on the cathode surface and the chemical reduction of polysulfide on the anode. The active shuttle phenomenon prolonged consequently the charge process, which reduce the cycling performance of the batteries

3.2 Influence of $LiNO_3$ as co-salt for the electrolyte

In 2008, Mikhaylik[31] studied the influence of lithium imide in a 50:50 ratio mixture of 1,3-dioxolane (DOL) and dimethoxyethane (DME) as well as in a solution of trifluoromethyl sulfonate. He postulated that N-O chemical bond was the responsible for inhibition of the shuttle mechanism. To demonstrate this; he tested salts containing the N-O bond like potassium nitrate, cesium nitrate, ammonium nitrate, potassium nitrite, and dinitro-toluene. The highest Coulombic efficiency and discharge capacity upon cycling were achieved with $LiNO_3$ concentrations between 0.2 M and 1.0 M. After this, several studies have shown the benefits of $LiNO_3$.[32–36] This additive or co-salt avoids large charging cycles, increasing the Coulombic efficiency to around 100%. This is attributed to elimination of the shuttle mechanisms due to the formation of a "protective" and Li^+ ion conductive layer on the anode surface. This layer is composed of Li_xNO_y and/or Li_xSO_y components[37] which prevents the reaction of polysulfides with lithium metal and thus it eliminates the shuttle effect during charge. In this section, $LiNO_3$ is used as a co-salt in 1 M $LiPF_6$ TEGDME electrolyte to stabilize the Coulombic efficiency and to increase the cyclability of the Li-S battery. The results of the electrochemical tests for different concentrations of $LiNO_3$ at 0.18 C-rate are summarized in Fig. 2.

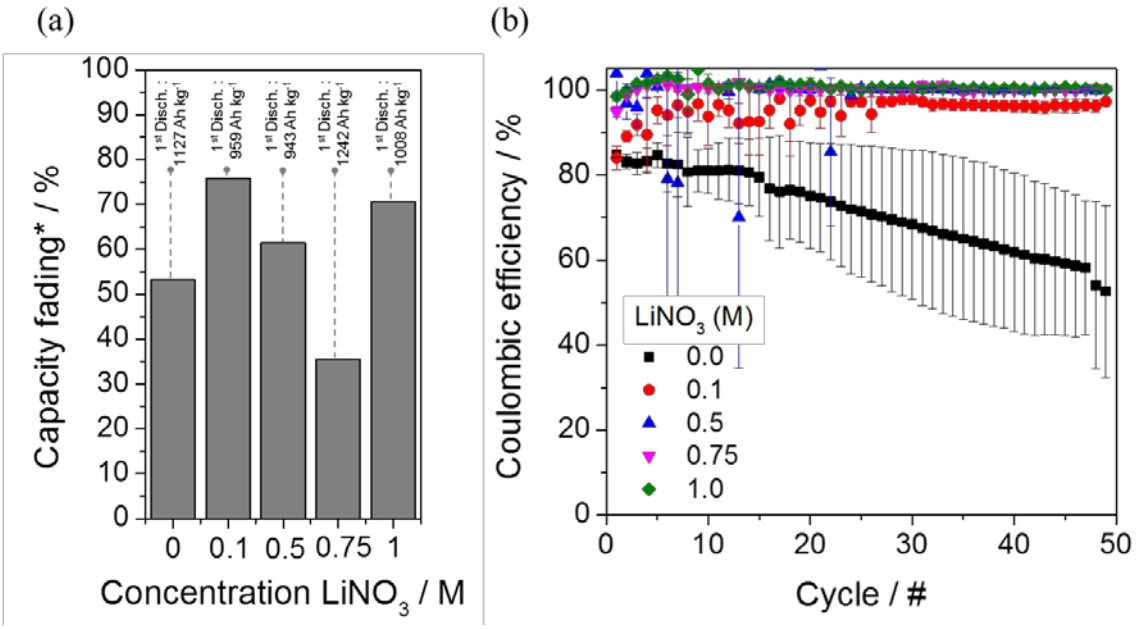

*Fig. 2 : Influence of concentration of $LiNO_3$ in the capacity fading of batteries after 50 cycles (a) and the Coulombic efficiency (b), tested at 0.18 C rate. *Capacity fading was calculated between cycle 1 and 50. The average and error bars are calculated based on the results of 3 tested batteries.*

The capacity fading is affected by the concentration of the co-salt and reaches a minimum of around 35% for 0.75 M $LiNO_3$ (Fig. 2 (a)). By further increase of concentration the capacity fading rises again. This last behavior may be explained by the formation of a thicker protective layer on the anode, which reduces the mobility of Li^+, and thus its availability for further reactions. Although the Coulombic efficiency reaches already values near to 100% with 0.1 M $LiNO_3$, by increasing the concentration the Coulombic efficiency is more stable (lower error bars, Fig. 2 (b)). Considering both the capacity fading and the Coulombic efficiency, the optimal concentration of $LiNO_3$ is found to be 0.75 M for this cell configuration.

To summarize, the improvements on capacity regarding cathode fabrication (Cathode I → Cathode II) and electrolyte modification (Cathode II without → with 0.75 M $LiNO_3$) are presented in Fig. 3. The reduction of sulfur particle size and its

homogenous distribution in the cathode layer influence mainly the initial discharge capacity (852 Ah kg_S^{-1} for Cathode I, 1127 Ah kg_S^{-1} for Cathode II). The co-salt reduces the shuttle mechanism which is reflected by the lower capacity fading and thus a higher capacity at the 50th cycle (527 Ah kg_S^{-1} Cathode II without $LiNO_3$, 800 Ah kg_S^{-1} with 0.75 M $LiNO_3$).

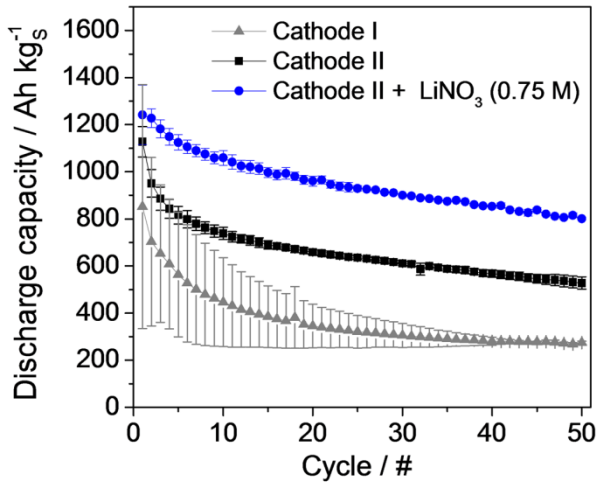

Fig. 3 : Improvements on the cyclability of the cell by modification of cathode and electrolyte. Test were performed at 0.18 C-rate. The average and error bars are calculated based on the results of 3 tested batteries.

Fig. 4 (a) shows the performance of the battery (Cathode II, Electrolyte: 0.75 M $LiNO_3$, 1 M $LiPF_6$ in TEGDME) when discharging at 0.18 C and 2 C up to 1000 cycles. As expected, the initial values of capacity are much lower for higher 2 C-rate. However, the charge capacity increases in the first cycles reaching it maximum at the 13th cycle. An explanation for this must be the lower dissolution of sulfur at the initial stages of discharge and lower crystallization of Li_2S at the end of discharge. The discharge reaction mechanism includes first the dissolution of sulfur in the electrolyte and second the reaction with Li ions to build up the polysulfides; when the discharge rate is fast, sulfur cannot dissolve completely and lower formation of polysulfides is

reached. Moreover, the crystallization of Li_2S is a lower process and this must favored after several cycles when polysulfides have been accumulated in the electrolyte.

The Coulombic efficiency maintains constant at values near to 100%, for both C-rates, confirming that the protective effect of $LiNO_3$ against the shuttle mechanisms prevails up to 1000 cycles. Some investigations have shown that the effect of $LiNO_3$ disappears at higher cycle number[34]; however, this is not observed in the cell tested through this work. The difference on capacity for cathode II (Fig. 4 and Fig. 5), with electrolyte: 0.75 M $LiNO_3$, 1 M $LiPF_6$ in TEGDME, tested at 0.18 C is caused by a difference of sulfur loading (-30%) because they were coated in different production lots. The standard deviation (average of the first 50 cycles) between both production lots was 59 Ah kg_S^{-1}.

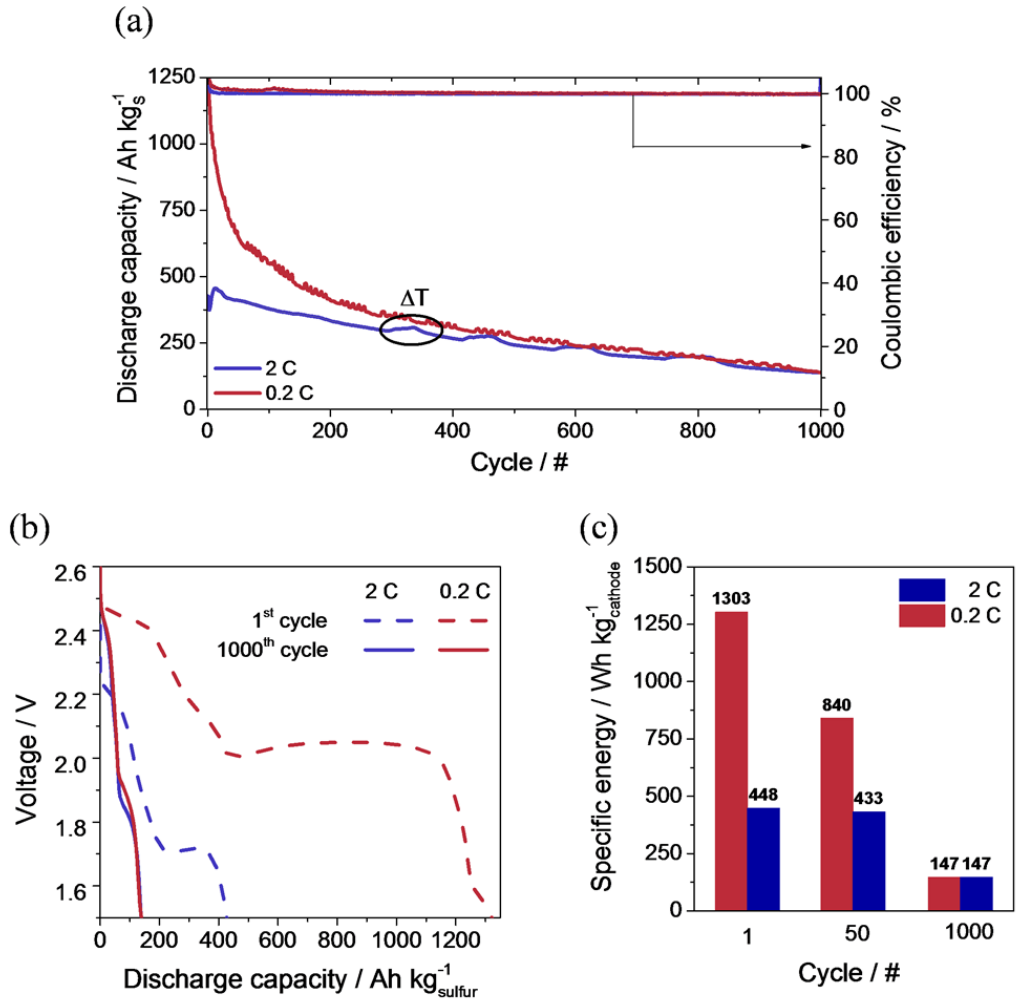

Fig. 4 : (a) Discharge capacity and Coulombic efficiency of Li-S batteries at 0.18 C and 2 C. The red inset in the picture shows an example of the variation of the capacity caused by changes in the environmental temperature during testing. The capacity increases 12 Ah kg$_S^{-1}$ per + 1°C (Temperature was measured outside the cell). (b) Comparison of discharge profile between batteries tested at 0.18 C and 2 C. (c) Specific energy density based on the cathode mass for cycle 1, 50, and 1000. Test show the results of one cell.

After 500 cycles both capacity curves meets and the capacity fading comes independent of the discharge rate. It is expected that inactive cores of S_8 or Li_2S are built up, and lower the utilization of active material in the subsequent cycles. Moreover, according with the similar discharge profile observed in Fig. 4 (b), the reaction mechanisms at different C-rates seems to be similar after 500 cycles. The first discharge plateau is shorter due to the lower amount of crystalline sulfur present in the charge state. Therefore, it is expected that most of the reactions occurs in the liquid phase; this means oxidation and reduction of polysulfides with less formation of S_8 or Li_2S. The average energy density of the cell calculated based on the total mass of cathode, is presented for cycle 1, 50, and 1000 in Fig. 4 (c).

3.3 Sulfur distribution and structural changes on the cathode

In previous work, we presented *in situ* XRD analysis of Li/S batteries[38]. It was demonstrated for the first time the formation of Li_2S during discharge during the first cycles. Moreover, the recrystallization of sulfur was also proved at the end of charge with an orientation of sulfur crystallites perpendicular to cathode surface. During charge, the reaction of Li_2S is slower compared with the recrystallization rate of sulfur. By the second discharge, almost 50% less crystalline Li_2S is formed compared with the first discharge. At the end of the second charge, the peaks of sulfur appear at the same positions, indicating a similar orientation of the particles as the one after the first charge. The formation of the amorphous phase which was not published provides important in-sight into the sulfur formation. For this reason, we evaluate now the amorphization of the cathode to complete the previous analysis[38].

A single line fitting for the amorphous phase combined with a refinement of the crystalline phase was performed. The background was fitted with a 1^{st} order function and the amorphous phase with a single Split-PseudoVoigt function (spv) located at the

maximum of the amorphous bump. The results show the changes of area of the amorphous bump during charge (Fig. 5 (a-d)). Before cycling almost no amorphous phase is present in the cathode, while discharge, this increases and almost triplicates it value at around 70% DOD. Next, when the formation of crystalline Li_2S increases[38], the amorphous phase reduces back but only to the double of its initial values. The amorphous phase built during discharge may be attributed to amorphous Li_2S or Li_2S_2. Until now there is no experimental evidence of the formation of Li_2S_2. Recently, Feng et al.[39] suggested that Li_2S_2 is electrochemically more active than Li_2S, and that its formation energy is higher than that of Li_2S plus S_8. Their calculations revealed that there are multiple crystal structures of Li_2S_2 and therefore, it almost always shows up as a mixture. Hence, it is difficult to evaluate using XRD.

During the initial period of the first charge, the amorphous phase remains constant and starts to increase at around 30% DOC, when almost 50% of the crystalline Li_2S already reacted to polysulfides. The highest amorphous area is measured between 50-80% DOC and then slightly decreases with the formation of crystalline sulfur. From this evidence, it is expected that the formation of crystalline sulfur follows similar transition processes than the slow solidification of melted sulfur (polymeric$_{(amorphous)}$ $\rightarrow$ monoclinic $\rightarrow$ orthorhombic). This would mean that first the sulfur chain molecule is build up according the reaction of Li_2S_8 ($xLi_2S_8 \rightarrow 2xLi + S_{8x(chain,\ amorphous)}$) and after the formation of crystalline sulfur occurs ($S_{8(chain,\ amorphous)} \rightarrow S_{8(cycle\ 1^{st}\ monoclinic,\ 2^{nd}\ orthorhombic)}$). This process seems not to be completely reversible, and only the crystalline phase reacts back in the next discharge process.

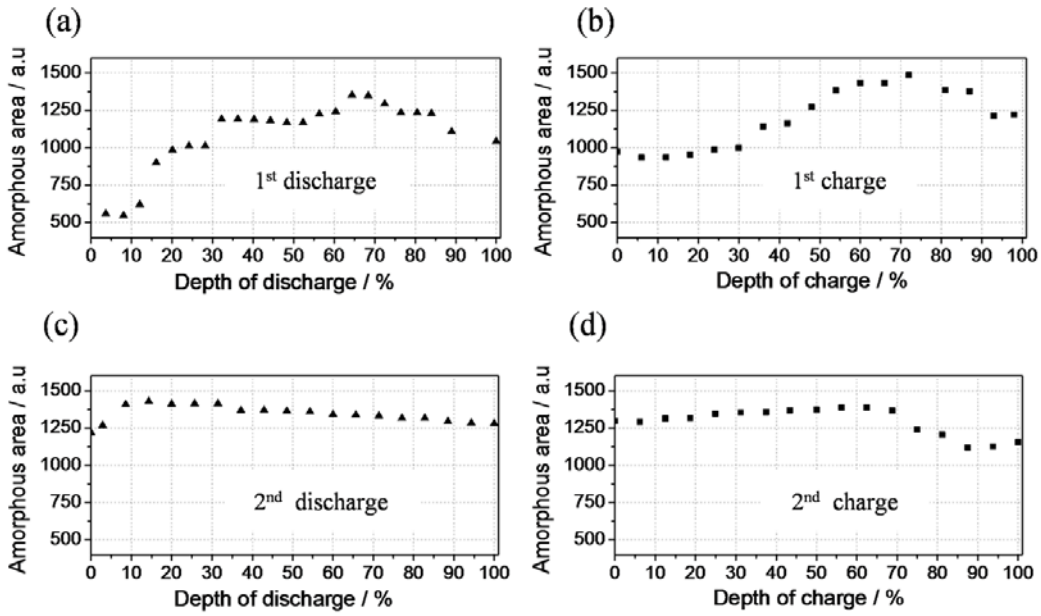

Fig. 5 : Semi-quantitative X-ray analysis for the first two discharges (a, c) and charge cycles (b, d) of a Li-S battery.

In the second cycle remains almost constant along the cycle. The presence of the amorphous phase is also observed after 100 cycles (Fig. 6). It is well known that polymeric sulfur does not dissolve in organic solvents like crystalline sulfur does. For this reason, it is expected that the loss of capacity is caused mostly by amorphous sulfur that build up as an isolating film over the conductive CB particles. Moreover, it is important to notice that after discharge the amorphous phase increases in 100% (from around 500 to 1000 a.u of amorphous area) and after this cycle it does not decrease any further. This means that the isolating layer formed during discharge does not disappear after charge; but rather increase in 25% due to the contribution of amorphous sulfur.

Fig. 6 illustrates the results of the XRD measurement at different positions in the cathode (according to Fig. 8). Before cycling, the cathode shows a homogenous

dispersion of sulfur, this is illustrated for the raster positions 1, 3, 7, 11, and 13. This implies that through the selected mixing procedure the cathode components are well mixed and that the coating procedure generates cathode with uniform thickness. In contrast, cathode after cycling show an inhomogeneous distribution of sulfur which is reflected by changes in the intensity of the reflections. Moreover, variation in the position of the peaks reveals changes of the orientation of the sulfur crystallites with the position.

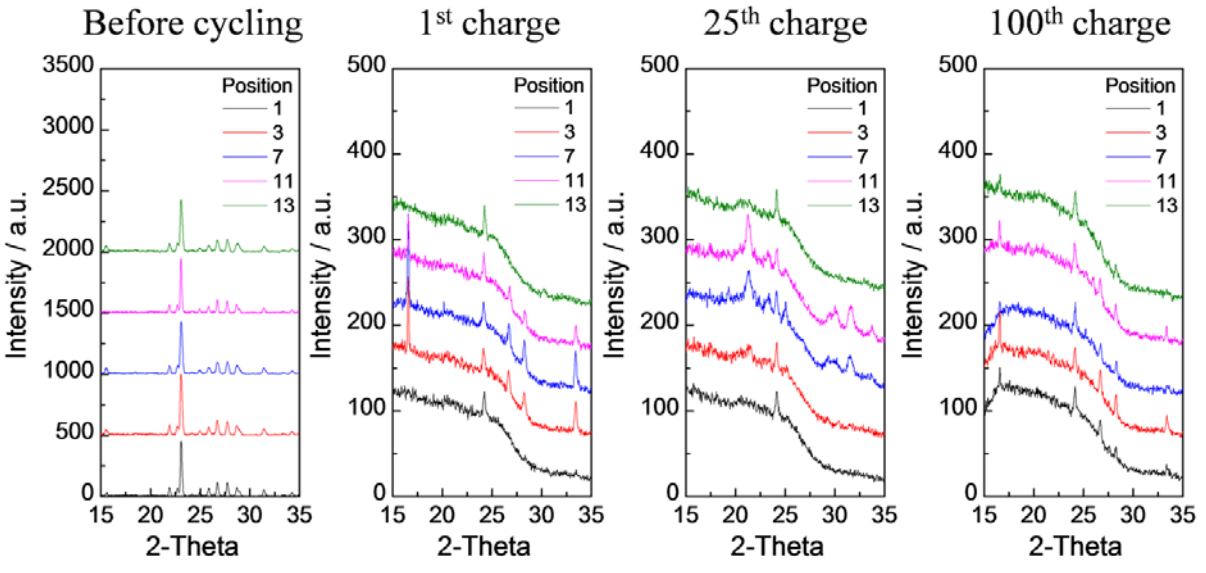

Fig. 6 : Diffraction data of the cathode before cycling, after the 1st, 25th, and 100th cycle for the positions 1, 3, 7, 11 and 13.

In Fig. 7 the integrated area of the sulfur reflexes are represented in the 13 positions of cathode II after the 1st cycle. The distribution of sulfur is inhomogeneous and the highest amount is located in the center of the cathode, in the side positions almost no crystalline sulfur was measured. The inhomogeneous distribution of sulfur in the cathode after cycling has been also seen using light microscopy (Fig. A.2-A3).

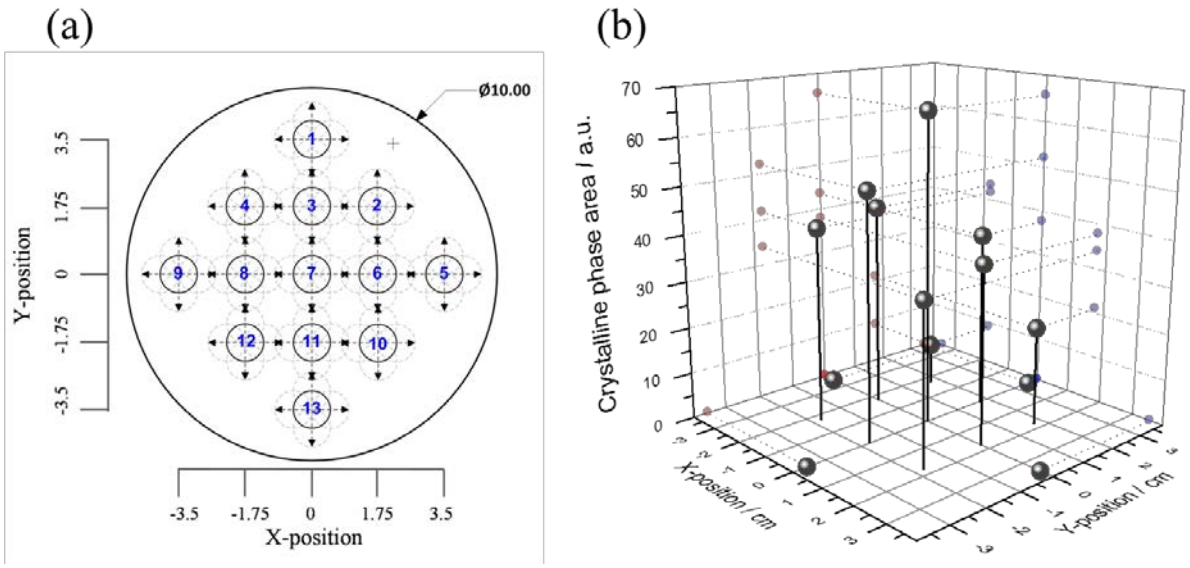

Fig. 7 : (a) Schematic raster grid for analyzing 10 mm diameter cathodes. 13 target positions were selected. Here the beam spots are illustrated as circles, although in reality they are elliptical and their size depends on the θ incident angle. (b)Spatial distribution of the sulfur crystalline phase after 1st charge.

3.4 Stability of binding

TG curves of the cathode before cycling are shown in Fig. 8. All the measurements were carried out under air atmosphere to detect CB and PVDF up to 800 °C and repeated for three samples. The first mass loss at 150 °C is related to sulfur oxidation, the slight decrease at around 400 °C to PDVF degradation, and at around 650 °C the oxidation of the carbon black particles occurs. TG/DSC diagrams of the cathode components can be found in Fig. A.6, A.7 and Table A.2. The oxidation temperature of transformation is in all cases lower than the characteristic temperature obtained for the components measured separately as a powder. This is explained by the fact that oxidation reactions occur at a slower rate in the cathode due to the binding between particles.

TG curves for cathodes after 1, 10, 50, and 100 cycles are illustrated in Fig. 8. As a complementary analysis to TG, the gas evolved during heating of sample was investigated with MS. The evolution of the mass number 64 (SO_2), 44 (CO_2), and 19 (F) is displayed in the curves. After cycling, the mass loss of sulfur occurs at lower temperature, SO_2 forms between 100-150 °C instead of 250-300 °C (before cycling). The shift of the oxidation of sulfur from 219 °C before cycling to ca. 120 °C after cycling is explained by the reduction of the crystallite size and structure after cycling, which increased the surface area of reaction. Furthermore, the crystallization of sulfur on the surface of the cathode and not in the bulk material may facilitate the reaction of sulfur with oxygen. The decrease in mass at around 120°C for cathodes after cycling is related not only to the mass of sulfur, but also to reaction products of electrolyte in air. This was proved by measuring a cathode after drying this with electrolyte (Fig. A.8). After cycling a decrease of the peak area for SO_2 is observed, this is correlated with the content of sulfur in the cathode. The loss of active material is caused by the incomplete reaction of polysulfides to sulfur during charge, as well by the loss of sulfur which deposits in the separator surface.

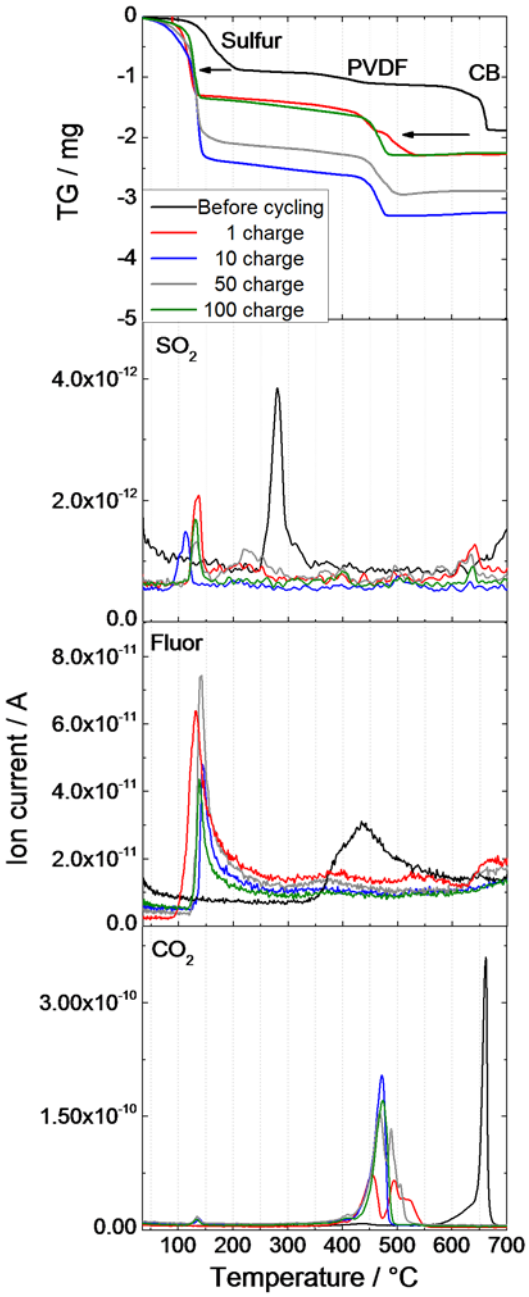

Fig. 8 : TG before cycling and after 1, 10, 50 and 100 cycles with the evolved gas analysis of SO_2 and CO_2.

The TG peak of PVDF is not distinguishable anymore after cycling. Moreover, the results of the MS reveals that the fluorine signal detected at around 400°C for the

cathode before cycling can no longer be detected after cycling. This may be a result of the decomposition of the binder by reaction with polysulfides during cycling.
Before cycling, CB particles oxidizes first slowly (small shoulder at 600°C) and then rapidly (sharp peak) at the temperature range of 600 – 700 °C. Contrary, oxidation occurs at 200°C lower for cathodes after cycling (660°C before cycling to 469°C after cycling (Table 1). These results suggest that the structure of CB is affected by the electrochemical cycling of the cathode; the binding of the CB particles in the structure may be partially destroyed, and this facilitates the oxidation process shown by the low oxidation temperatures in the TG measurements. In addition, the oxidation process after cycling occurs in some cases in several steps: see double peaks in MS of CB i.e. cycle 1 and 50. Nevertheless, the appearance of one or several peaks could not be attributed to a specific cycle of the battery´s life.

Table 1: Changes in oxidation temperature of cathode components.

4. Conclusions

The use of wet powder-spraying allows the fabrication of homogenous sulfur-composite layers. However, the use of large amount of solvents is a disadvantage, and a solvent recuperation system should be implemented in case of industrial applications. Improvements on the mixing and milling processes showed that well-dispersed and small sulfur particles, surrounded by CB particles, improves the sulfur utilization during the first cycles, which results in an increased of battery performance from 275 to 528 Ah kg_S^{-1} after 50 cycles. Nevertheless, the capacity fading of the battery is still high (47 %) and it is caused among others by the low Coulombic efficiency generated by the shuttle mechanisms. This can be improved by the utilization of $LiNO_3$ as co-salt in the electrolyte. With this electrolyte additive and cell configuration discharge

capacities of 800 Ah kg_S^{-1} were achieved (50 cycles, at 0.18 C-rate). Further studies will be focused in the protection of this cathode with protective layers for the retention of active material [26,32,40–43].

The appearance of an amorphous phase is revealed during cycling. The amount of this phase increases during the first discharge/charge and remains almost stable in the further cycles. This may be associated to the formation of amorphous S during charge and amorphous Li_2S or Li_2S_2 during discharge. The change in structure of sulfur already shown using XRD, it is confirmed in the TG curves: the formation of small crystallite or deposition of active material on the surface shift the oxidation process from 219 °C (before cycling) to 130 °C (after cycling). In addition, the loss of the TG-Peak of PVDF after cycling is attributed to its degradation and this may affect the binding between the CB and S particles during cycling. A drastically reduction of the oxidation temperature of CB from 660 °C (before cycling) to 469 °C (after cycling) reveals that the conductive material is also altered by the electrochemical cycling. This reduction may be explained by the destruction of the CB structure, which is important for the electron transport in the cell.

Appendix A. Supplementary data

Supplementary data associated with this article can be found, in the online version, at

References

[1] X. Ji, L.F. Nazar, Advances in Li–S batteries, J. Mater. Chem. 20 (2010) 9821.

[2] A. Manthiram, Y. Fu, Y.-S. Su, Challenges and Prospects of Lithium-Sulfur Batteries., Acc. Chem. Res. 46 (2012) 1125–1134.

[3] Z. Wei Seh, W. Li, J.J. Cha, G. Zheng, Y. Yang, M.T. McDowell, et al., Sulphur-TiO2 yolk-shell nanoarchitecture with internal void space for long-cycle lithium-sulphur batteries., Nat. Commun. 4 (2013) 1331–1336.

[4] J. Xie, J. Yang, X. Zhou, Y. Zou, J. Tang, S. Wang, et al., Preparation of three-dimensional hybrid nanostructure-encapsulated sulfur cathode for high-rate lithium sulfur batteries, J. Power Sources. 253 (2014) 55–63.

[5] S.-C. Han, M.-S. Song, H. Lee, H.-S. Kim, H.-J. Ahn, J.-Y. Lee, Effect of Multiwalled Carbon Nanotubes on Electrochemical Properties of Lithium/Sulfur Rechargeable Batteries, J. Electrochem. Soc. 150 (2003) A889–A893.

[6] J.-W. Choi, G. Cheruvally, D.-S. Kim, J.-H. Ahn, K.-W. Kim, H.-J. Ahn, Rechargeable lithium/sulfur battery with liquid electrolytes containing toluene as additive, J. Power Sources. 183 (2008) 441–445.

[7] J. Sun, Y. Huang, W. Wang, Z. Yu, A. Wang, K. Yuan, Preparation and electrochemical characterization of the porous sulfur cathode using a gelatin binder, Electrochem. Commun. 10 (2008) 930–933.

[8] X. He, J. Ren, L. Wang, W. Pu, C. Jiang, C. Wan, Expansion and shrinkage of the sulfur composite electrode in rechargeable lithium batteries, J. Power Sources. 190 (2009) 154–156.

[9] B. Zhang, C. Lai, Z. Zhou, X.P. Gao, Preparation and electrochemical properties of sulfur–acetylene black composites as cathode materials, Electrochim. Acta. 54 (2009) 3708–3713.

[10] D. Marmorstein, T.H. Yu, K.A. Striebel, F.R. Mclarnon, J. Hou, E.J. Cairns, Electrochemical performance of lithiumrsulfur cells with three different polymer electrolytes, J. Po. 89 (2000) 219–226.

[11] J. Shim, K.A. Striebel, E.J. Cairns, The Lithium/Sulfur Rechargeable Cell, J. Electrochem. Soc. 149 (2002) A1321–A1325.

[12] C. Barchasz, J.-C. Leprêtre, F. Alloin, S. Patoux, New insights into the limiting parameters of the Li/S rechargeable cell, J. Power Sources. 199 (2012) 322–330.

[13] J.L. Wang, J. Yang, J.Y. Xie, N.X. Xu, Y. Li, Sulfur–carbon nano-composite as cathode for rechargeable lithium battery based on gel electrolyte, Electrochem. Commun. 4 (2002) 499–502.

[14] J. Wang, L. Liu, Z. Ling, J. Yang, C. Wan, C. Jiang, Polymer lithium cells with sulfur composites as cathode materials, Electrochim. Acta. 48 (2003) 1861–1867.

[15] L. Ji, M. Rao, H. Zheng, L. Zhang, Y. Li, W. Duan, et al., No Title, J. Am. Chem. Soc. 133 (2011) 18522–18525.

[16] B. Ding, C. Yuan, L. Shen, G. Xu, P. Nie, Q. Lai, et al., Chemically tailoring the nanostructure of graphene nanosheets to confine sulfur for high-performance lithium-sulfur batteries, J. Mater. Chem. A. 1 (2013) 1096–1101.

[17] X. Ji, K.T. Lee, L.F. Nazar, A highly ordered nanostructured carbon-sulphur cathode for lithium-sulphur batteries., Nat. Mater. 8 (2009) 500–6.

[18] B. Zhang, X. Qin, G.R. Li, X.P. Gao, Enhancement of long stability of sulfur cathode by encapsulating sulfur into micropores of carbon spheres, Energy Environ. Sci. 3 (2010) 1531–1537.

[19] X. Li, Y. Cao, W. Qi, L. V. Saraf, J. Xiao, Z. Nie, et al., Optimization of mesoporous carbon structures for lithium–sulfur battery applications, J. Mater. Chem. 21 (2011) 16603.

[20] V. Maurice, A.W. Hassel, P. Marcus, S.-R. Chen, Y.-P. Zhai, G.-L. Xu, et al., Ordered mesoporous carbon/sulfur nanocomposite of high performances as cathode for lithium–sulfur battery, Electrochim. Acta. 56 (2011) 9549–9555.

[21] Z. Wang, S. Zhang, L. Zhang, R. Lin, X. Wu, H. Fang, et al., Hollow spherical carbonized polypyrrole/sulfur composite cathode materials for lithium/sulfur cells with long cycle life, J. Power Sources. 248 (2014) 337–342.

[22] N. Jayaprakash, J. Shen, S.S. Moganty, A. Corona, L.A. Archer, Porous hollow carbon@sulfur composites for high-power lithium-sulfur batteries., Angew. Chemie Int. Ed. 50 (2011) 5904–5908.

[23] Y. Fu, Y.-S. Su, A. Manthiram, Sulfur-Polypyrrole Composite Cathodes for Lithium-Sulfur Batteries, J. Electrochem. Soc. 159 (2012) A1420–A1424.

[24] N. Ding, S.W. Chien, T.S.A. Hor, Z. Liu, Y. Zong, Key parameters in design of lithium sulfur batteries, J. Power Sources. 269 (2014) 111–116.

[25] J. Hassoun, M. Agostini, A. Latini, S. Panero, Y.-K. Sun, B. Scrosati, Nickel-Layer Protected, Carbon-Coated Sulfur Electrode for Lithium Battery, J. Electrochem. Soc. 159 (2012) A390.

[26] Y.-S. Su, A. Manthiram, Lithium–sulphur batteries with a microporous carbon paper as a bifunctional interlayer, Nat. Commun. 3 (2012) 1166.

[27] Q. Tang, Z. Shan, L. Wang, X. Qin, K. Zhu, J. Tian, et al., Nafion coated sulfur–carbon electrode for high performance lithium–sulfur batteries, J. Power Sources. 246 (2014) 253–259.

[28] N.A. Cañas, K. Hirose, B. Pascucci, N. Wagner, K.A. Friedrich, R. Hiesgen, Investigations of lithium–sulfur batteries using electrochemical impedance spectroscopy, Electrochim. Acta. 97 (2013) 42–51.

[29] N.A. Cañas, D.N. Fronczek, N. Wagner, A. Latz, K.A. Friedrich, Experimental and Theoretical Analysis of Products and Reaction Intermediates of Lithium–Sulfur Batteries, J. Phys. Chem. C. 118 (2014) 12106–12114.

[30] http://www.basytec.de/prospekte/CTS%202013_03.pdf, (n.d.).

[31] Y. V. Mikhaylik, Electrolytes for lithium sulfur cells, U.S. Patent US7842421 B2, 2008.

[32] S. Xiong, K. Xie, Y. Diao, X. Hong, Properties of surface film on lithium anode with LiNO3 as lithium salt in electrolyte solution for lithium–sulfur batteries, Electrochim. Acta. 83 (2012) 78–86.

[33] X. Liang, Z. Wen, Y. Liu, M. Wu, J. Jin, H. Zhang, et al., Improved cycling performances of lithium sulfur batteries with LiNO3-modified electrolyte, J. Power Sources. 196 (2011) 9839–9843.

[34] M. Hagen, E. Quiroga-González, S. Dörfler, G. Fahrer, J. Tübke, M.J. Hoffmann, et al., Studies on preventing Li dendrite formation in Li–S batteries by using pre-lithiated Si microwire anodes, J. Power Sources. 248 (2014) 1058–1066.

[35] S. Xiong, K. Xie, Y. Diao, X. Hong, Characterization of the solid electrolyte interphase on lithium anode for preventing the shuttle mechanism in lithium–sulfur batteries, J. Power Sources. 246 (2014) 840–845.

[36] H.S. Kim, T. Jeong, N. Choi, Y. Kim, The cycling performances of lithium – sulfur batteries in TEGDME / DOL containing LiNO 3 additive, Ionics (Kiel). 19 (2013) 1795–1802.

[37] D. Aurbach, E. Pollak, R. Elazari, G. Salitra, C.S. Kelley, J. Affinito, On the Surface Chemical Aspects of Very High Energy Density, Rechargeable Li–Sulfur Batteries, J. Electrochem. Soc. 156 (2009) A694.

[38] N.A. Cañas, S. Wolf, N. Wagner, K.A. Friedrich, In-situ X-ray diffraction studies of lithium–sulfur batteries, J. Power Sources. 226 (2013) 313–319.

[39] Z. Feng, C. Kim, A. Vijh, M. Armand, K.H. Bevan, K. Zaghib, Unravelling the role of Li2S2 in lithium-sulfur batteries: A first principles study of its energetic and electronic properties, J. Power Sources. (2014).

[40] H. Schneider, A. Garsuch, A. Panchenko, O. Gronwald, N. Janssen, P. Novák, Influence of different electrode compositions and binder materials on the performance of lithium – sulfur batteries, J. Power Sources. 205 (2012) 420–425.

[41] G.-C. Li, G.-R. Li, S.-H. Ye, X.-P. Gao, A Polyaniline-Coated Sulfur/Carbon Composite with an Enhanced High-Rate Capability as a Cathode Material for Lithium/Sulfur Batteries, Adv. Energy Mater. 2 (2012) 1238–1245.

[42] Z. Lin, Z. Liu, W. Fu, N.J. Dudney, C. Liang, Phosphorous Pentasulfide as a Novel Additive for High-Performance Lithium-Sulfur Batteries, Adv. Funct. Mater. 23 (2012) 1064–1069.

[43] R. Elazari, G. Salitra, Y. Talyosef, J. Grinblat, C. Scordilis-Kelley, A. Xiao, et al., Morphological and Structural Studies of Composite Sulfur Electrodes upon Cycling by HRTEM, AFM and Raman Spectroscopy, J. Electrochem. Soc. 157 (2010) A1131–A1138.